

Observation of Reactor Electron Antineutrino Disappearance in the RENO Experiment

J. K. Ahn,⁷ S. Chebotaryov,⁶ J. H. Choi,⁴ S. Choi,¹⁰ W. Choi,¹⁰ Y. Choi,¹² H. I. Jang,¹¹ J. S. Jang,² E. J. Jeon,⁸ I. S. Jeong,² K. K. Joo,² B. Kim,² B. C. Kim,² H. S. Kim,¹ J. Y. Kim,² S. B. Kim,¹⁰ S. H. Kim,⁷ S. Y. Kim,⁷ W. Kim,⁶ Y. D. Kim,⁸ J. Lee,¹⁰ J. K. Lee,⁷ I. T. Lim,² K. J. Ma,⁸ M. Y. Pac,⁴ I. G. Park,⁵ J. S. Park,¹⁰ K. S. Park,⁹ J. W. Shin,¹⁰ K. Siyeon,³ B. S. Yang,¹⁰ I. S. Yeo,² S. H. Yi,¹² and I. Yu¹²

(RENO Collaboration)

¹*Department of Physics, Chonbuk National University, Jeonju 561-756, Korea*

²*Department of Physics, Chonnam National University, Gwangju, 500-757, Korea*

³*Department of Physics, Chung Ang University, Seoul 156-756, Korea*

⁴*Department of Radiology, Dongshin University, Naju, 520-714, Korea*

⁵*Department of Physics, Gyeongsang National University, Jinju, 660-701, Korea*

⁶*Department of Physics, Kyungpook National University, Daegu, 702-701, Korea*

⁷*Department of Physics, Pusan National University, Busan, 609-735, Korea*

⁸*Department of Physics, Sejong University, Seoul 143-747, Korea*

⁹*Division of General Education, Seokyeong University, Seoul, 136-704, Korea*

¹⁰*Department of Physics and Astronomy, Seoul National University, Seoul 151-742, Korea*

¹¹*Department of Fire Safety, Seoyeong University, Gwangju, 500-742, Korea*

¹²*Department of Physics, Sungkyunkwan University, Suwon, 440-746, Korea*

The RENO experiment has observed the disappearance of reactor electron antineutrinos, consistent with neutrino oscillations, with a significance of 6.3 standard deviations. Antineutrinos from six 2.8 GW_{th} reactors at Yonggwang Nuclear Power Plant in Korea, are detected by two identical detectors located at 294 m and 1383 m, respectively, from the reactor array center. In the 229 day data-taking period of 11 August 2011 to 26 March 2012, the far (near) detector observed 17102 (154088) electron antineutrino candidate events with a background fraction of 4.9% (2.7%). A ratio of observed to expected number of antineutrinos in the far detector is $0.922 \pm 0.010(\text{stat.}) \pm 0.008(\text{syst.})$. From the deficit, we find $\sin^2 2\theta_{13} = 0.103 \pm 0.013(\text{stat.}) \pm 0.011(\text{syst.})$ based on a rate-only analysis.

PACS numbers: 14.60.Pq, 29.40.n, 28.50.Hw, 13.15.+g

We report a definitive measurement of a neutrino oscillation mixing angle, θ_{13} , based on the disappearance of electron antineutrinos emitted from six reactors. It is the only undetermined one out of the three mixing angles in the Pontecorvo-Maki-Nakagawa-Sakata matrix [1, 2]. Searches for θ_{13} in the neutrino oscillations have obtained only its upper limits [3–9]. CHOOZ [3] and MINOS [5] experiments set the most stringent limit, $\sin^2 2\theta_{13} < 0.15$ (90% C.L.). Recently, indications of non-zero θ_{13} have been reported by two accelerator appearance experiments, T2K [10] and MINOS [11], and by a reactor disappearance experiment of Double Chooz [12]. Global analyses of all available neutrino oscillation data have indicated central values of $\sin^2 2\theta_{13}$ between 0.05 and 0.1 (see e.g. [13, 14]). During preparation of this paper, Daya Bay reported observation of a non-zero value for θ_{13} [15].

Reactor experiments with a baseline distance of ~ 1 km, can neglect the disappearance of $\bar{\nu}_e$ driven by θ_{12} and Δm_{21}^2 , and thus clearly measure the mixing angle θ_{13} based on the survival probability of electron antineutrinos,

$$P_{\text{survival}} \approx 1 - \sin^2 2\theta_{13} \sin^2(1.267\Delta m_{31}^2 L/E), \quad (1)$$

where E is the energy of antineutrinos in MeV, and L is the baseline distance in meters between reactor

and detector. The well measured value of $\Delta m_{32}^2 = (2.32_{-0.08}^{+0.12}) \times 10^{-3} \text{ eV}^2$ [16] can substitute the Δm_{31}^2 in Eq. (1).

The detection methods and setup of RENO experiment are discussed in details elsewhere [17]. In this Letter, only the components relevant to this measurement are reviewed. A symmetric arrangement of the reactors and the detectors is useful for minimizing the complexity of this measurement. Two identical antineutrino detectors are located at 294 m and 1383 m, respectively, from the center of reactor array to allow a relative measurement by comparing the measured neutrino rates. A measured far-to-near ratio of antineutrinos can considerably reduce several systematic errors coming from uncertainties in the reactor neutrino flux, target mass, and detection efficiency. The relative measurement is independent of correlated uncertainties and helps in minimizing uncorrelated reactor uncertainties. The angle θ_{13} is obtained by finding a reduction of the observed reactor neutrino fluxes in the far detector, relative to the expectation from the near measurement. The near detector is located inside a restricted area of the nuclear power plant, quite close to the reactors to make an accurate measurement of the antineutrino fluxes before their oscillations. The six pressurized water reactors with each maximum ther-

mal output of 2.8 GW_{th} (reactors 3, 4, 5, and 6) or 2.66 GW_{th} (reactors 1 and 2) are lined up in roughly equal distances and span $\sim 1.3 \text{ km}$. The far (near) detector is under a 450 (120) m.w.e. (meters of water equivalent) rock overburden.

The positions of two detectors and six reactors are surveyed with GPS and total station to determine the baseline distances between detector and reactor to an accuracy of less than 10 cm. Reactor neutrino fluxes at detector are obtained by calculating the reduction effect of the baseline distances to a precision of much better than 0.1%. We found negligible effect on calculation of the reactor neutrino flux from the spatial distribution of fuel assemblies in the core. Individual contribution of each reactor to the reactor antineutrino fluxes at both detectors is found at their full powers, as listed in Table I. The reactor-flux weighted baseline is 408.56 m for the near detector, and 1443.99 m for the far detector.

TABLE I. Fractional antineutrino contribution of reactor to detector considering flux reduction due to the baseline distance.

Reactor	Near Detector	Far Detector
1	6.78%	13.73%
2	14.93%	15.74%
3	34.19%	18.09%
4	27.01%	18.56%
5	11.50%	17.80%
6	5.58%	16.08%

The reactor $\bar{\nu}_e$ is detected through inverse beta decay (IBD) reaction, $\bar{\nu}_e + p \rightarrow e^+ + n$. Detectors based on hydrocarbon liquid scintillator (LS) provide free protons as a target. Only $\bar{\nu}_e$ with energy above 1.81 MeV participates in the IBD reaction. The coincidence of a prompt positron signal and a delayed signal from neutron capture by Gadolinium (Gd) provides a distinctive IBD signature.

The RENO detector (Fig. 1) consists of a main inner detector (ID) and an outer veto detector (OD). The main detector is contained in a cylindrical stainless steel vessel of 5.4 m in diameter and 5.8 m in height which houses two nested cylindrical acrylic vessels. The innermost 25 mm thick acrylic vessel of 2.75 m in diameter and 3.15 m in height holds 18.6 m^3 (16 t) of $\sim 0.1\%$ Gd doped LS as a neutrino target. It is surrounded by a γ -catcher region, useful for recovering γ -rays escaping from the target region, with a 60 cm thick layer and 33.2 m^3 (29 t) of Gd unloaded LS inside an outer 30 mm thick acrylic vessel of 4.0 m in diameter and 4.4 m in height. The acrylic vessels holding organic liquids are made of casted polymethylmethacrylate (PMMA) plastic which transmits up to 92% of visible light at 3 mm thickness and reflects about 4% from the surfaces [18]. Outside the γ -catcher is the buffer region, a 70 cm thick layer filled

with 65 t mineral oil. It provides shielding from radioactivity of photomultipliers (PMTs) and of the surrounding rock. Light signals emitted from particles interacting in ID are detected by 354 10-inch Hamamatsu R7081 PMTs, mounted on the inner wall of the stainless steel, providing 14% surface coverage. Outside the ID is the OD with a 1.5 m thick layer filled with highly purified water to identify events coming from outside by their Cherenkov radiation and to shield against ambient γ -rays and neutrons from the surrounding rock. The OD is equipped with 67 10-inch R7081 water-proof PMTs mounted on the wall of the veto vessel. The whole surfaces of OD are covered with Tyvek sheets to increase the light collection.

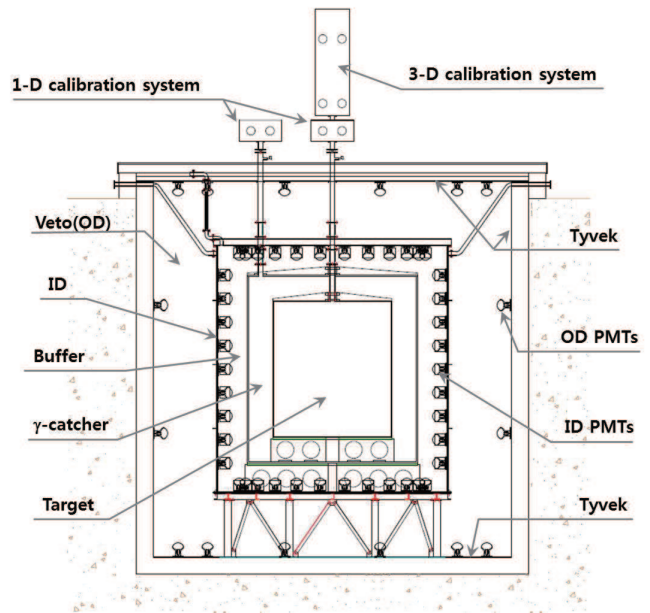


FIG. 1. A schematic view of the RENO detector. The near and far detectors are identical.

The LS is developed and produced as a mixture of linear alkyl benzene (LAB), 3 g/l of PPO, and 30 mg/l of bis-MSB. LAB ($C_nH_{2n+1}-C_6H_5$, $n=10\sim 13$) is an organic solvent with a high flash point (130°C), a good light yield, and a large attenuation length. A Gd-carboxylate complex using TMHA was developed for the best Gd loading efficiency into LS and its long term stability [19]. Gd-LS and LS are made and filled into the detectors carefully to ensure that the near and far detectors are identical.

The results presented in this Letter are based on data taken from 11 August 2011 to 26 March 2012, for total 229 days. During this period, all six reactors were mostly on at full power, and reactors 1 and 2 were off for a month each because of fuel replacement. Data-taking efficiency is high, 88% for the near detector and 97% for the far detector.

Event triggers are formed by the number of PMTs with signals above a ~ 0.3 photoelectron (pe) threshold (NHIT). An event is triggered and recorded if the ID NHIT is larger than 90, corresponding to 0.5~0.6 MeV well below the 1.02 MeV as the minimum energy of an IBD positron signal, or if the OD NHIT is larger than 10. The ID trigger only rate is 70 Hz (105 Hz) and the OD trigger rate is 60 Hz (520 Hz) at the far (near) detector. The ID trigger provides no loss of IBD candidates. The OD trigger inefficiency is negligible for cosmic muons which could introduce spallation neutrons and any other cosmogenic backgrounds. The readout electronics records the charge and time of all the PMT hits at 60 kHz with no dead time, and a trigger decision is made at the software level.

The detectors are calibrated using radioactive sources and cosmic-ray induced background samples. Radioisotopes of ^{137}Cs , ^{68}Ge , ^{60}Co , and ^{252}Cf are periodically deployed in the target and γ -catcher by a step motorized pulley system in a glove box. The system deploys a source only along the vertical direction. A motorized robot-arm system is developed to deploy a source in various positions in the target. The detector stability in energy response is regularly monitored using cosmic-ray produced neutron captures on H and Gd.

The event energy is measured based on the total charge (Q_{tot}) in pe, collected by the PMTs and corrected for gain variation. The energy calibration constant of 250 pe per MeV is determined by the peak energies of various radioactive sources deployed at the center of the target. An energy dependent calibration constant is applied to include a slight non-linear energy response of the detector. The energy scale correction to constant calibration varies from -1% to +3% for 0.7~10.0 MeV. A spallation-neutron produces a 2.2 MeV γ -ray by a capture on H and ~ 8.0 MeV γ 's by a capture on Gd. The peak energies of those samples are also used to determine the energy scale. The energy response is found to be stable within 1% over the time period of taking data, used in this analysis. The obtained energy resolution is $(5.9/\sqrt{E(\text{MeV})} + 1.1)\%$, common for both detectors.

Monte Carlo detector simulation (MC), based on GEANT4 [20], is used to study the detector response and to obtain the detection efficiency. The MC includes measured optical properties of LS such as emission, absorption, re-emission, refraction, etc [19]. Comparisons between data and MC are used to estimate the systematic errors due to uncertainties of energy and detection efficiency.

In this analysis, an IBD event requires a delayed signal from a neutron capture on Gd, and thus the fiducial volume naturally becomes the whole target vessel region without any vertex position cuts. There could be spill-in IBD events, occurring outside the target and producing a neutron capture on Gd in the target, to enhance the detection efficiency. Conversely, spill-out IBD events lower

the detection efficiency.

The following criteria are applied to select IBD candidate events: (1) $Q_{max}/Q_{tot} < 0.03$ to eliminate PMT flasher events and external γ -ray events where Q_{max} is the maximum charge of a PMT; (2) a cut rejecting events within a 1 ms window following a cosmic muon traversing ID if the muon deposit energy (E_μ) is larger than 70 MeV, or if E_μ is between 20 MeV and 70 MeV for OD NHIT > 50 ; (3) a cut rejecting events within a 10 ms window following a cosmic muon traversing ID if E_μ is larger than 1.5 GeV; (4) $0.7 \text{ MeV} < E_p < 12.0 \text{ MeV}$; (5) $6.0 \text{ MeV} < E_d < 12.0 \text{ MeV}$, (6) $2 \mu\text{s} < \Delta t_{e+n} < 100 \mu\text{s}$ where E_p (E_d) is the energy of the prompt (delayed) event and $\Delta t_{e+n} = t_d - t_p$ is the time difference between the prompt and delayed signals; (7) a multiplicity cut rejecting correlated coincidence pairs if they are accompanied with any preceding ID or OD trigger within a 100 μs window before their prompt candidate.

Applying the IBD selection cuts yields 17102 (154088) candidate events or 77.02 ± 0.59 (800.8 ± 2.0) events/day for a live time of 222.06 (192.42) days in the far (near) detector. The vertex distribution is found to be uniform inside the target region.

In the final data samples, uncorrelated (accidentals) and correlated (fast neutrons from outside of ID, stopping muon followers, and β -n emitters from $^9\text{Li}/^8\text{He}$) background events remain after the selection cuts. We have avoided applying a long-time (> 10 ms) veto cut after a cosmic muon which results in a substantial loss of signals. The background sample of cosmic muon induced $^9\text{Li}/^8\text{He}$ events is selected separately for accurate subtraction from the IBD final data set.

TABLE II. Event rates of the observed candidates and the estimated background.

Detector	Near	Far
Selected events	154088	17102
Total background rate (per day)	21.81 ± 6.67	3.77 ± 0.52
IBD rate after background subtraction (per day)	778.99 ± 6.96	73.25 ± 0.79
DAQ Live time (days)	192.42	222.06
Detection efficiency (ϵ)	0.647 ± 0.014	0.745 ± 0.014
Accidental rate (per day)	4.30 ± 0.06	0.68 ± 0.03
$^9\text{Li}/^8\text{He}$ rate (per day)	12.51 ± 6.67	2.12 ± 0.52
Fast neutron rate (per day)	5.00 ± 0.13	0.97 ± 0.06

The uncorrelated background is accidental coincidences from random association of a prompt-like event due to radioactivity (10.6Hz in the far detector) and a delayed-like neutron capture (26.8/hour in the far detector). The remaining rate in the final sample is estimated by measuring the rates of prompt- and delayed-like events after applying all the selection cuts but the cut (6), and calculating the probability of random association in the Δt window for IBD selection, leading to 4.30 ± 0.06 (near)

or 0.68 ± 0.03 (far) events per day. An independent check is made by extracting the accidental contribution to the final IBD sample by a random spatial correlation, obtained from prompt and delayed candidates separated by more than 2 meters at distance, and finds a consistent background rate.

The ${}^9\text{Li}/{}^8\text{He}$ β -n emitters are caused mostly by energetic muons because of their increasing production cross sections in the carbon with muon energy [21–23]. Their signature is a prompt β signal, and accompanied by a delayed neutron capture with a half-life time of 178 ms (${}^9\text{Li}$) or 119 ms (${}^8\text{He}$). The background rate is estimated from a sample prepared by a delay coincidence between an energetic (deposited $E_\mu > 0.5$ GeV) muon and its following IBD-like pair of events. The measured mean lifetime of ${}^9\text{Li}/{}^8\text{He}$ candidates is consistent with that of ${}^9\text{Li}$. The ${}^9\text{Li}/{}^8\text{He}$ β -n background rate in the final sample is obtained as 12.51 ± 6.67 (near) or 2.12 ± 0.52 (far) events per day by fitting the delay time distribution with an observed mean decay time of ~ 250 ms. The ${}^9\text{Li}/{}^8\text{He}$ spectrum is also obtained to be used for background subtraction.

An energetic neutron entering ID can interact in the target to produce a recoil proton before being captured on Gd. The fast moving neutrons are produced by cosmic muons traversing the surrounding rock and the detector. The background rate is estimated by extrapolating the spectral shape of $12 \text{ MeV} < E_p < 30 \text{ MeV}$, to the IBD signal region, assuming a flat spectrum of the fast neutron background. The estimated fast neutron background is 5.00 ± 0.13 (near) or 0.97 ± 0.06 (far) events per day. The total background rate is estimated to be 21.81 ± 6.67 (near) or 3.77 ± 0.52 (far) events per day, as presented in Table II.

The common detector efficiency, without consideration of inefficiency due to the muon veto and multiplicity cuts, is estimated to be $(76.5 \pm 1.4)\%$ using MC and data (see Table III). The trigger inefficiency is found to be negligible for the IBD signal with an analysis threshold of 0.7 MeV. Both prompt energy and flasher cuts are almost fully (99.8%) efficient. The fraction of neutron captures on Gd is evaluated to be $(85.5 \pm 0.7)\%$ using MC and ${}^{252}\text{Cf}$ source data. The Δt_{e+n} cut efficiency is obtained to be $(92.1 \pm 0.5)\%$ from MC and data. The fraction of neutron captures on Gd accepted by the 6.0 MeV cut is $(95.2 \pm 0.5)\%$. The overall efficiency of finding a delayed signal as an IBD candidate pair is $(75.0 \pm 1.0)\%$. The spill-in IBD events result in the increase of detection efficiency by 2.2%. The enhancement is due to the neutrons from IBD interactions near and outside the target and entering into the target, and estimated using MC.

The fractional loss $\delta_{\mu\text{-veto}}$ of IBD events due to the muon veto is calculated as $(11.30 \pm 0.04)\%$ (near) or $(1.36 \pm 0.02)\%$ (far), by summing the spent time in vetoing events after muons. The fractional loss δ_{multi} of IBD events due to the multiplicity cut is calculated as

$(4.61 \pm 0.04)\%$ (near) or $(1.22 \pm 0.07)\%$ (far), based on the ID trigger rate and the veto window from an IBD prompt candidate. The uncertainties of the muon veto and multiplicity cuts come from variations of muon and trigger rates due to a fluctuation of energy threshold, and are not common in the both detectors. The efficiency of detecting IBD events is found to be $(64.7 \pm 1.4)\%$ (near) or $(74.5 \pm 1.4)\%$ (far), as presented in Table III.

TABLE III. Detection efficiency for the IBD events.

	Efficiency	
Prompt energy cut	$(99.8 \pm 0.1)\%$	
Flasher cut	$(99.8 \pm 0.1)\%$	
Gd capture fraction	$(85.5 \pm 0.7)\%$	
Delayed energy cut	$(95.2 \pm 0.5)\%$	
Time coincidence cut	$(92.1 \pm 0.5)\%$	
Spill-in	$(102.2 \pm 1.0)\%$	
Common	$(76.5 \pm 1.4)\%$	
	Near	Far
Muon veto loss ($\delta_{\mu\text{-veto}}$)	$(11.30 \pm 0.04)\%$	$(1.36 \pm 0.02)\%$
Multiplicity cut loss (δ_{multi})	$(4.61 \pm 0.04)\%$	$(1.22 \pm 0.07)\%$
Total	$(64.7 \pm 1.4)\%$	$(74.5 \pm 1.4)\%$

This analysis is independent of absolute neutrino fluxes due to two identically performing detectors at near and far locations from reactors. The absolute uncertainties of the efficiencies are correlated between the two detectors. Only differences between the two identical detectors are taken as uncorrelated uncertainties. The systematic uncertainties are summarized in Table IV.

TABLE IV. Systematic uncertainties in the reactor neutrino detection.

Reactor		
	Uncorrelated	Correlated
Thermal power	0.5%	–
Fission fraction	0.7%	–
Fission reaction cross section	–	1.9%
Reference energy spectra	–	0.5%
Energy per fission	–	0.2%
Combined	0.9%	2.0%
Detection		
	Uncorrelated	Correlated
IBD cross section	–	0.2%
Target protons	0.1%	0.5%
Prompt energy cut	0.01%	0.1%
Flasher cut	0.01%	0.1%
Gd capture ratio	0.1%	0.7%
Delayed energy cut	0.05%	0.5%
Time coincidence cut	0.01%	0.5%
Spill-in	0.03%	1.0%
Muon veto cut	0.02%	0.02%
Multiplicity cut	0.04%	0.06%
Combined (total)	0.2%	1.5%

Uncorrelated relative uncertainties are estimated by comparing the two detectors. The IBD differential cross section is taken from Ref. [24]. The total number of free protons in the target is 1.189×10^{30} with an uncertainty of 0.5%, by measurements of the LS weight and the composition of hydrogen. The relative energy scale difference between the detectors is obtained to be 0.2% by comparing the peak energy values of several radioactive calibration sources, IBD delayed events, and cosmic muon induced spallation-neutron captures on H and Gd. The energy scale difference finds the relative uncertainty in the efficiency of the delayed energy (E_d) cut to be 0.1% using data. Gd-LS was made, divided equally, and filled into the two detectors to ensure that the Gd concentration and the target protons of near and far detectors are identical. Considering the uncertainty in dividing Gd-LS, the difference of the target protons is less than 0.1%. The difference in measured neutron capture time between the detectors is less than $0.2 \mu s$, corresponding to Gd concentration difference less than 0.1%. The relative uncertainty of Gd capture ratio is less than 0.1% accordingly. The rest relative uncertainties are close to 0.01%, and the combined uncertainty common to the both detector is 0.2%. More detailed discussion on the systematic uncertainties will be presented in the future publication.

The reactor antineutrinos are mainly emitted from the fissions of four isotopes (^{235}U , ^{239}Pu , ^{238}U , ^{241}Pu). The antineutrino flux depends on thermal power, fission fractions of the four isotopes, energy released per fission, and fission and capture cross-section. The uncertainty associated with the thermal power, provided by the power plant, is 0.5% per core, fully correlated among reactors [25]. The relative fission contributions of the four main isotopes are evaluated and provided for a fuel cycle, with 4~10% uncertainties, using a reactor simulation code of Westinghouse ANC [26]. The uncertainties of the fission fraction simulation contribute 0.7% of the $\bar{\nu}_e$ yield per core to the uncorrelated uncertainty. The associated antineutrino flux is computed based on the $\bar{\nu}_e$ yield per fission [27] and the fission spectra [28–32], leading to a 1.9% correlated uncertainty which causes little effect on the results. The thermal energy released per fission is given in Ref. [33], and its uncertainty results in a 0.2% correlated uncertainty. We assume a negligible contribution of the spent fuel to the uncorrelated uncertainty in this analysis.

All the reactors were mostly in steady operation at the full power during the data-taking period, but the reactor 2 was off for a month, September 2011, and reactor 1 was off from February 23 2012 to change the fuels. Fig. 2 presents the measured daily rate of IBD candidates after background subtraction, at near and far detectors. The expected rates assuming no oscillation, obtained from the weighted fluxes by the thermal power and the fission fractions of each reactor and its baseline to each detector, are shown for comparison.

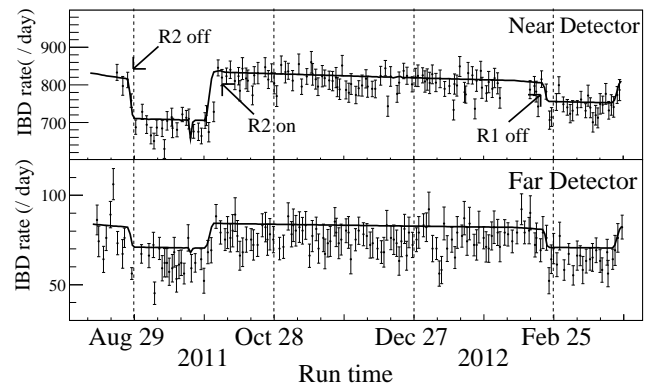


FIG. 2. Measured daily-average rates of reactor neutrinos after background subtraction in the near and far detectors as a function of running time. The solid curves are the predicted rates of no oscillation with their normalizations corrected by the best fit result in determining $\sin^2 2\theta_{13}$.

The ratio of measured to expected events in the far detector is

$$R = 0.922 \pm 0.010(\text{stat.}) \pm 0.008(\text{syst.}),$$

finding a clear deficit. To determine the value of $\sin^2 2\theta_{13}$ from the deficit, a χ^2 with pull terms on the correlated systematic uncertainties [34] is used,

$$\chi^2 = \sum_{d=N,F} \frac{\left[N_{obs}^d + b_d - (1 + \xi_d) \sum_{r=1}^6 (1 + f_r) N_{exp}^{d,r} \right]^2}{N_{obs}^d} + \sum_{d=N,F} \left(\frac{\xi_d^2}{\sigma_d^{\xi^2}} + \frac{b_d^2}{\sigma_d^b} \right) + \sum_{r=1}^6 \left(\frac{f_r}{\sigma_r} \right)^2, \quad (2)$$

where N_{obs}^d is the number of observed IBD candidates in each detector after background subtraction, $N_{exp}^{d,r}$ is the number of expected events from neutrino flux, detection efficiency, neutrino oscillations, and contribution from the r -th reactor to each detector determined by baselines and reactor fluxes. The uncorrelated reactor uncertainty is 0.9% (σ_r), the uncorrelated detection uncertainty is 0.2% (σ_d^{ξ}), as listed in Table IV, and σ_d^b is the background uncertainty listed in Table III. f_r , ξ_d , and b_d are corresponding pull parameters. Note that the correlated uncertainties of detector and reactor are not included in this analysis.

The best-fit value obtained is

$$\sin^2 2\theta_{13} = 0.103 \pm 0.013(\text{stat.}) \pm 0.011(\text{syst.}) \quad (3)$$

excluding the no-oscillation hypothesis at 6.3 standard deviation.

The fast neutron and $^9\text{Li}/^8\text{He}$ backgrounds produced by cosmic muons depend on the detector sites having different overburdens. Therefore, their uncertainties are the largest contribution to the uncorrelated error in this

analysis, and change the systematic error by 0.00x at the best-fit value.

Fig. 3 shows the χ^2 distribution as a function of $\sin^2 2\theta_{13}$, and the ratios of the measured reactor neutrino events, relative to the expected without oscillation at both detectors. We observe a clear deficit of 7.8% for the far detector, and of 1.7% for the near detector, concluding a definitive observation of reactor antineutrino disappearance consistent with neutrino oscillations. The survival probability due to neutrino oscillation at the best-fit value is given by the curve.

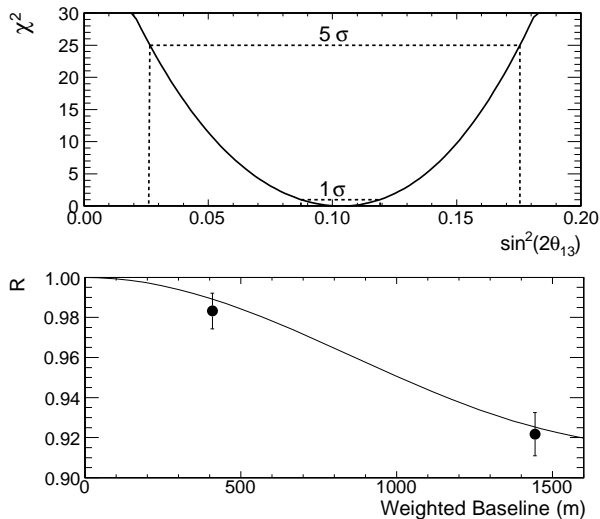


FIG. 3. The χ^2 distribution as a function of $\sin^2 2\theta_{13}$. Bottom: Ratio of the measured reactor neutrino events relative to the expected with no oscillation. The expected signal is adjusted with the best-fit normalization. The curve represents the oscillation survival probability at the best fit, as a function of the flux-weighted baselines.

The observed spectrum of IBD prompt signals in the far detector is compared to the expected from the measurement in the near detector as shown in Fig. 4. The spectra of prompt signals exhibit those of reactor antineutrinos, and are obtained after background subtraction as shown in the inset. The disagreement of the spectra provides further evidence of neutrino oscillation.

In summary, RENO has observed reactor antineutrinos using two identical detectors with 16 ton Gd-loaded liquid scintillator each, and a 229 day exposure to total 16.5 GW_{th} reactors. In the far detector, a clear deficit of 7.8% is found by comparing a total of 17102 observed events with an expectation from the near detector measurement assuming no oscillation. Based on the deficit, a rate-only analysis obtains $\sin^2 2\theta_{13} = 0.103 \pm 0.013(\text{stat.}) \pm 0.011(\text{syst.})$. The neutrino mixing angle θ_{13} is measured with a significance of 6.3 standard deviation.

The RENO experiment is supported by the Ministry

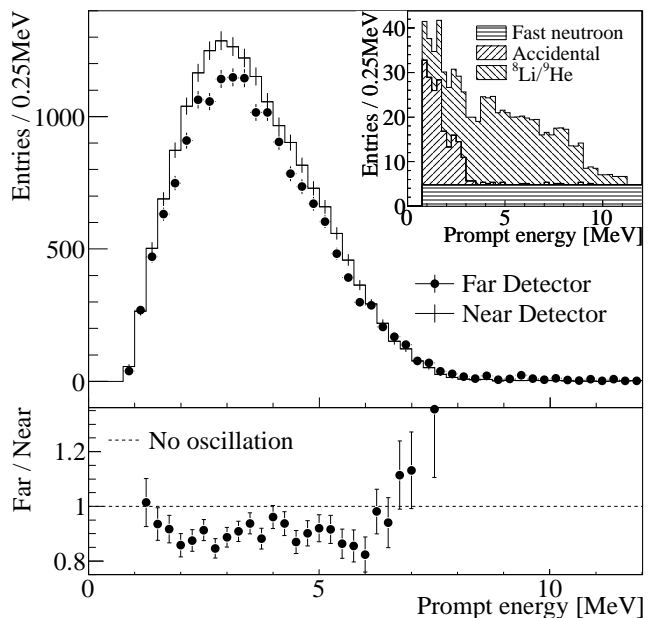


FIG. 4. Measured energy spectrum of the prompt signals from the reactor neutrinos in the far detector compared with the no-oscillation prediction from the measurements in the near detector. The background shown in the inset is subtracted for the spectra. The background fraction is 4.9% (2.7%) for far (near) detector. Errors are statistical uncertainties only. Bottom: The ratio of the measured spectrum of far detector to the no-oscillation prediction.

of Education, Science and Technology of Korea and the Korea Neutrino Research Center selected as a Science Research Center by the National Research Foundation of Korea. We gratefully acknowledge the cooperation of the Yonggwang Nuclear Power Site and the Korea Hydro & Nuclear Power Co., Ltd. (KHNP). We thank KISTI's providing computing and network resources through GSDC, and all the technical and administrative people who greatly helped in making this experiment possible.

-
- [1] B. Pontecorvo, Zh. Eksp. Theo. Fiz. **34**, 247 (1957) [Sov. Phys. JETP **7**, 172 (1958)].
 - [2] Z. Maki, M. Nakagawa, and S. Sakata, Prog. Theor. Phys. **28**, 870 (1962).
 - [3] M. Apollonio *et al.* (Chooz Collaboration), Phys. Lett. **B466**, 415 (1999); Eur. Phys. J. C **27**, 331 (2003).
 - [4] F. Boehm *et al.* (Palo Verde Collaboration), Phys. Rev. Lett. **84**, 3764 (2000).
 - [5] P. Adamson *et al.* (MINOS Collaboration), Phys. Rev. D **82**, 051102 (2010).
 - [6] S. Yamamoto *et al.* (K2K Collaboration), Phys. Rev. Lett. **96**, 181801 (2006).
 - [7] R. Wendell *et al.* (Super-Kamiokande Collaboration), Phys. Rev. D **81**, 092004 (2010).

- [8] B. Aharmim *et al.* (SNO Collaboraiton), Phys. Rev. C **81**, 055504 (2010).
- [9] A. Gando *et al.* (KamLAND Collaboration), Phys. Rev. D **83**, 052002 (2011).
- [10] K. Abe *et al.* (T2K Collaboration), Phys. Rev. Lett. **107**, 041801 (2011).
- [11] P. Adamson *et al.* (MINOS Collaboration), Phys. Rev. Lett. **107**, 181802 (2011).
- [12] Y. Abe *et al.* (Double Chooz Collaboration), Phys. Rev. Lett. **108**, 131801 (2012).
- [13] G. L. Fogli *et al.*, Phys. Rev. D **84**, 053007 (2011).
- [14] T. Schwetz *et al.*, New J. Phys. **13**, 109401 (2011).
- [15] F. P. An *et al.* (Daya Bay Collaboration) (2012), arXiv:hep-ex/1203.1669.
- [16] P. Adamson *et al.* (MINOS Collaboration), Phys. Rev. Lett. **106**, 181801 (2011).
- [17] J.K. Ahn, *et al.* (RENO Collaboration) (2010), arXiv:hep-ex/1003.1391.
- [18] K. S. Park, *et al.*, Construction and Properties of Acrylic Vessels in the RENO Detector, in preparation.
- [19] J. S. Park, *et al.*, Production and Optical Properties of Gd-loaded Liquid Scintillator for the RENO Neutrino Detector, in preparation.
- [20] S. Agostinelli *et al.*, Nucl. Instr. and Meth. **A506**, 250 (2003).
- [21] T. Hagner *et al.*, Astropart. Phys. **14**, 33 (2000).
- [22] D. R. Tilley *et al.*, Nucl. Phys. **A745**, 155 (2004).
- [23] S. Abe *et al.* (KamLAND Collaboration), Phys. Rev. C **81**, 025807 (2010).
- [24] P. Vogel and J. F. Beacom, Phys. Rev. D **60**, 053003 (1999).
- [25] S. F. E. Tournu *et al.*, EPRI 2001.1001470, Palo Alto, CA. (2001).
- [26] ANC: A Westinghouse Advanced Nodal Computing Code, Westinghouse Report WCAP-10965-P-A(P) (1986).
- [27] Y. Declais *et al.*, Phys. Lett. **B338**, 383 (1994).
- [28] W. G. K. Schreckenbach, G. colvin and F. von Feilitzsch, Phys. Lett. **B160**, 325 (1985).
- [29] F. von Feilitzsch and K. Schreckenbach, Phys. Lett. **B118**, 162 (1982).
- [30] A. A. Hahn *et al.*, Phys. Lett. **B218**, 365 (1989).
- [31] T. Mueller *et al.*, Phys. Rev. C **83**, 054615 (2011).
- [32] P. Huber, Phys. Rev. C **84**, 024617 (2011) [Erratum-ibid, **85**, 029901(E) (2012)].
- [33] V. Kopeikin *et al.*, Phys. Atom. Nucl. **67**, 1892 (2004).
- [34] D. Stump *et al.*, Phys. Rev. D **65**, 014012 (Appendix B) (2001).